11th International Symposium on Turbulence and Shear Flow Phenomena (TSFP11)
Southampton, UK, July 30 to August 2, 2019

TOWARD THE DEVELOPMENT OF A PREDICTIVE MODEL OF THE ROUGHNESS SUBLAYER FLOW

Karin Blackman
LHEEA, UMR 6598 CNRS
Centrale Nantes, 44300 Nantes, France
karin.blackman@ec-nantes.fr

Laurent Perret
LHEEA, UMR 6598 CNRS
Centrale Nantes, 44300 Nantes, France
laurent.perret@ec-nantes.fr

Romain Mathis
Institut de Mécanique des Fluides de Toulouse (IMFT)
Université de Toulouse, CNRS, 31400 Toulouse, France
romain.mathis@imft.fr

ABSTRACT

The non-linear interactions between large-scale momentum regions and small-scale structures induced by the presence of the roughness have been studied in boundary layers consisting of staggered cube arrays with plan area packing density of 6.25%, 25% or 44.4%. The measurements, consisting of hot-wire anemometry, were conducted at two Reynolds numbers in each of the canopy configurations. The canopy configuration is shown to have a significant influence on all parameters of the predictive model close to the roughness elements which is a result of the characteristics of the small-scale structures induced by the presence of the cubes. Several tests of the predictive model have been undertaken, demonstrating the good capability of the model to reproduce accurately spectra and statistics up to the 4^{th} order. The model must be however calibrated for each type of canopy flow regime.

INTRODUCTION

The rough-wall turbulent boundary layer contains coherent structures such as large-scale regions of high or low momentum that are present above the canopy within the inertial layer and shear layers that form within the roughness sublayer and contain small-scale structures induced by the presence of the roughness. Within the smooth-wall a non-linear mechanism of amplitude modulation has been shown to exist between the large-scale structures in the inertial layer and the small-scales close to the wall (Mathis, 2011, 2009). The amplitude modulation was shown to increase with increasing Reynolds number (Re) as large-scale structures become more turbulent (Mathis, 2009). Amplitude modulation has also been confirmed to exist in the rough-wall and although the modulation was shown to differ quantitatively from the smooth-wall the nature of the mechanism remained the same (Squire, 2016). Recently, the most energetic large-scale momentum regions in an urban-type boundary layer were shown to interact non-linearly with the small-scale structures induced by the presence of the roughness (Blackman & Perret, 2016). The study of amplitude modulation in the smooth-wall boundary layer has led to the development of a predictive model for the near-wall fluctuations using a large-scale boundary layer signal (Mathis, 2011). The application of this predictive model has been expanded to a rough-wall consisting of sand-roughness (Squire, 2016) and has recently been improved using Spectral Linear Stochastic Estimation (SLSE) (Baars, 2016). However, this predictive model has yet to be applied to an urban-type rough-wall boundary layer. The effect of the roughness configuration used to generate a rough-wall boundary layer has been studied extensively including its influence on the non-linear interactions (Blackman *et al.*, 2018). It was found using skewness decomposition and spatio-temporal correlations that the configuration of the roughness had a non-negligible influence of the non-linear interactions. Recently, Perret (2019) studied the influence of canopy flow regime and Reynolds number on the characteristics of the scale-decomposed velocity fluctuations using staggered cube arrays with plan area packing densities of 6.25%, 25% and 44.4%. Although the Reynolds number was shown to have a negligible effect on the characteristics of the large-scale fluctuations the skimming flow regime was shown to result in near-canopy large-scales that contributed more to the variance suggesting that a stronger correlation exists between the inertial layer and the roughness sublayer as the canopy flow becomes less important. Here, rough-wall boundary layers consisting of cube roughness with various plan area packing densities are used to investigate *(i)* the influence of the canopy geometry on the interaction between the outer large-scales and the small-scales near the canopy, *(ii)* the influence of the canopy configuration and Reynolds number on the parameters of the predictive model, and *(iii)* the applicability of the predictive model, in its current form, to urban-type boundary layer.

EXPERIMENTAL SETUP

The experiments were conducted in the atmospheric boundary layer wind tunnel of the LHEEA (Nantes), which has a working section dimensions of 2 m (width) $\times$ 2 m (height) $\times$ 24 m (length). Five 800 mm vertical tapered spires and a 200 mm high solid fence were used to initiate the boundary layer. These turbulence generators were then followed by the roughness elements which consisted

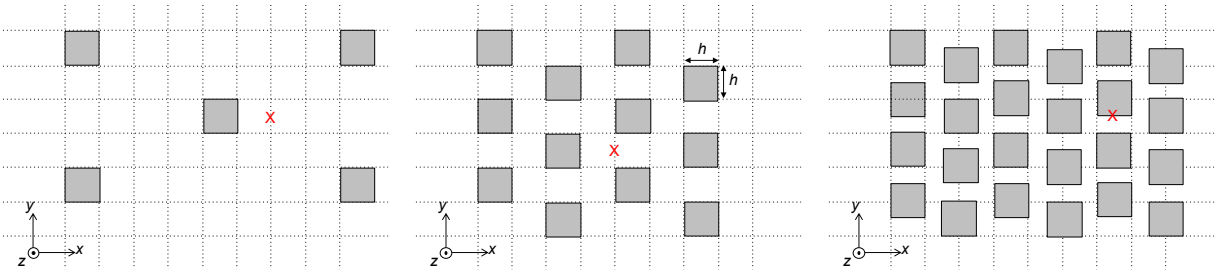

Figure 1. Investigated canopy configurations with, *(left)* λ_p = 6.25%, *(centre)* λ_p = 25% and *(right)* λ_p = 44% where the red cross (×) is the location of the hot-wire measurement location.

of staggered cubes with height of 50 mm. For further details related to the wind tunnel facility and set-up the reader is referred to Blackman & Perret (2016). Three different canopy configurations with plan area packing densities (the ratio between the area of the surface occupied by the roughness elements and the total surface area) of 6.25%, 25% or 44.4% were studied (Fig. 1) corresponding to the three flow regimes, isolated wake, wake interaction and skimming flows, respectively (Grimmond & Oke, 1999). Finally, the experiments were performed at two freestream velocities U_e of 5.7 and 8.8 m/s, resulting in a total of 6 flow configurations. Characteristics of each flow regimes are give in Table 1.

Table 1. Characteristics of the boundary layers. The coloured symbols chart will be used in all the following figures.

	$\lambda_p(\%)$	U_e (m/s)	δ/h	Re_τ	h^+
○	6.25	5.65	22.4	29700	1330
●	6.25	8.80	21.5	45500	2110
△	25	5.77	22.7	32400	1430
▲	25	8.93	22.1	49900	2260
□	44.4	5.62	23.2	27300	1170
■	44.4	8.74	22.1	40700	1840

The flow measurements were conducted using two synchronised hot-wire probes in order to investigate the relationships between the lower part of the boundary layer and the logarithmic region (Fig. 2). The first was a fixed hot-wire probe at a the wall-normal location $z/h = 5$ (*i.e.* within the inertial layer), while the second probe was moved to 13 different heights between $z/h = 1.25$ and $z/h = 4$. The hot-wire measurements were conducted at a frequency of 10 kHz for a period of 24 000 δ/U_e and calibration was performed at the beginning of measurement set by placing the probes in the freestream flow. Further details about this dataset, extended analysis of velocity profiles, statistics and spectral content can be found in Perret (2019), and Basley *et al.* (2019).

THE PREDICTIVE MODEL

The predictive model developed by Mathis (2011) has the ability to predict the fluctuating streamwise velocity in the inner region from an outer region input. Recently,

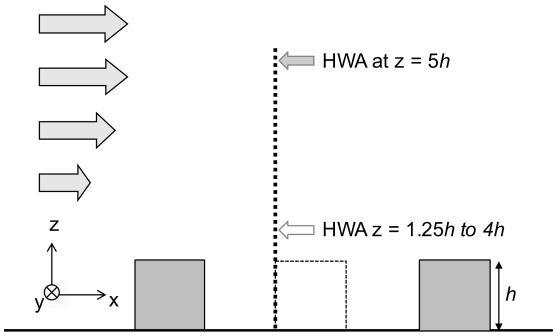

Figure 2. HWA measurement set-up.

an alternative approach to this model has been proposed by Baars (2016) who rewrite the model as

$$u_p^+(z,t) = u^*(z,t)(1+\Gamma(z)u_L^+(z,t-\tau_a)+u_L^+(z,t) \quad (1)$$

Here, u_p^+ is the predicted statistically representative streamwise fluctuating velocity signal obtained at the inner location z and u_L^+ is the fluctuating large-scale streamwise velocity signal and the only input into the model. u^* is the universal time series that corresponds to the universal signal that would exist if there were no large-scale influence. Here, the superscript $+$ denotes a normalization of the velocity fluctuation using u_τ. The universal signal, u^*, and coefficient Γ are determined using a calibration method involving two-point measurements of the streamwise velocity fluctuations. The model consists of two parts with the first part describing the amplitude modulation by the large-scale outer layer structures and the second part which models the superposition of these large-scale structures. To obtain the large-scale component in the inner region, $u_L^+(z,t)$, Baars (2016) propose a refined procedure using Spectral Linear Stochastic Estimation (SLSE) based on the coherence that exist between the outer and inner signals (*i.e.* the large-scale effect felt near the wall). The same method is applied here and the reader is referred to Baars (2016) and Perret (2019) for further details about this filter procedure. Once u_L^+ has been determined the model is calibrated in order to determine the universal signal u^* and the location-dependent coefficient Γ. A time shift, τ_a, has been introduced to this new model in the large-scale component that appears only in the modulation term to account for the phase-shift that exist between the local (inner) large-scale component and the large-scale envelope of the amplitude modulated small-scales (Guala *et al.*, 2011; Baars *et al.*, 2015). It is estimated as the time shift of the maximum of the cross-correlation between the outer layer signal, u_o^+, and the large-scale signal

produced from the SLSE method, u_L^+. The model calibration is conducted using the synchronised two-point hot-wire measurements described in previous section at each of the 13 wall-normal locations. To derive the model's parameters u^* and Γ, the small-scale signal of the inner layer is obtained using:

$$u_S^+(z,t) = u^+(z,t) - u_L^+(z,t) \tag{2}$$

This signal represents the fluctuations that are uncorrelated with the outer layer large-scale structures. As described, the universal signal is the signal that exists in the absence of any influence of the large-scales and u_S^+ does not include any superposition effect, but does include amplitude modulation effects. Therefore, to find u^* equation 3 is used where Γ is solved by iterative search such that u^* does not involve any amplitude modulation. Here, the absence of amplitude modulation is defined using the skewness as it has been previously shown by Blackman & Perret (2016) that the non-linear term $\overline{u_L u_S^2}$ is directly related to amplitude modulation. Therefore u^* constitutes no amplitude modulation when

$$\overline{u_L(z,t-\tau_a)u^{*2}} = \overline{u_L(z,t-\tau_a)\left(\frac{u_S^+(z,t)}{1+\Gamma(z)u_L^+(z,t-\tau_a)}\right)^2} = 0 \tag{3}$$

For every wall-normal measurement position, equation 3 is solved iteratively to obtain $\Gamma(z)$ where u^* is minimally modulated by $u_L^+(z,t-\tau_a)$ and u^* is then computed using this coefficient.

Scale decomposition

In the case of atmospheric surface layer developing over large roughness elements, the cubical obstacles induce energetic structures with typical frequencies smaller than that of the near-smooth wall turbulence. The range of the structures is close to those attributed to the large-scale structures developing in the outer region, which explained why the outer and inner peaks are rarely separated. It should be emphasised that the absence of a clear separation between inner and outer peaks does not mean that large-scale influence does not exist, but rather that a significant overlapping exist between the different coherent structures interacting with each others (Perret, 2019). This is the reason why the scale separation methods based on a SLSE approach has been favoured (Baars, 2016) against the classical Fourier approach used in Mathis (2009). Using the method, we are now able to extract the large- (u_L^+) and small-scale (u_S^+) signals from the raw near-wall velocity signal (u_{NW}^+) at each of the moving HWA probe wall-normal locations, and in each of the six cases using a transfer function. A comparison of their statistics up to the fourth order is given in figure 3, only for the flow configuration $\lambda_p = 25\%$ at Re_τ =32 400. Results are similar for all other cases not shown here. It can be observed that the small-scales capture the majority of the energy in the inner-layer while the large-scales contribution becomes important only in the outer layer. The skewness appeared to be exclusively driven by the small-scales, while the contribution of the large-scale is close to zero. The kurtosis of the raw signal is shown to be a result of both u_L^+ and u_S^+. A direct insight of the amplitude modulation effect can be obtained by comparing the u_S^+ and u^* signals, as the universal signal is a typical small-scale signal without any large-scale influence. Therefore, the only difference between both signals is that u_S^+ is modulated whereas u^* is not. It can be observed that the only difference between both signals lies in the skewness profile (Fig. 3, middle). In the absence of amplitude modulation the magnitude of skewness of u^* is significantly lower throughout the boundary layer, which is consistent with the close relationship between amplitude modulation and skewness highlighted by Mathis *et al.* (2011). They further showed that the non-linear term $\overline{u_L^+ u_S^{+2}}$ of the decomposed skewness provides

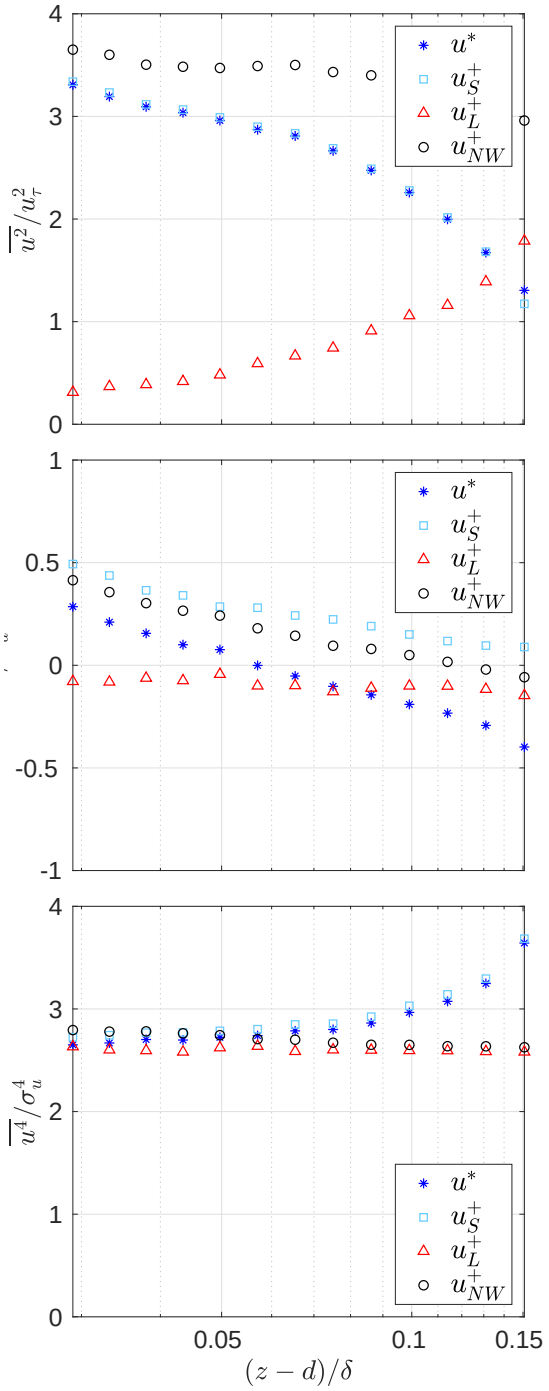

Figure 3. Comparison of u^*, u_L^+, u_S^+ and u_{NW}^+ statistics, *(top)* variance, *(middle)* skewness and *(bottom)* kurtosis, for configuration with $\lambda_p = 25\%$ at Re_τ =32 400.

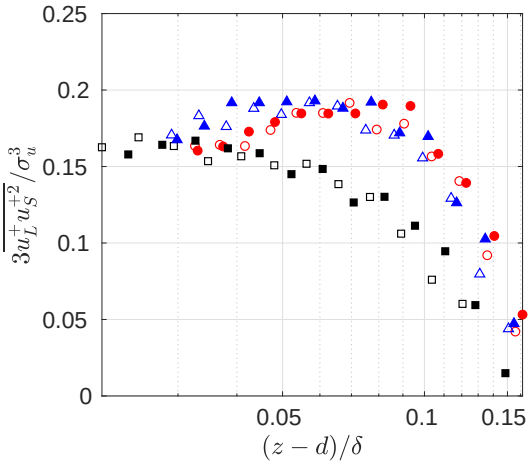

Figure 4. Wall-normal evolution of the non-linear term $3\overline{u_L^+ u_S^{+2}}$ of the decomposed skewness profile.

a good estimation of the degree of modulation, which is shown in figure 4 for all of the six configurations. It is clear that the skimming flow ($\lambda_p = 44.4\%$) is significantly modified at both Reynolds numbers compared to the isolated wake and wake interference flows. This result can be explained by the fact that this flow configuration has a finest roughness sublayer and the small-scale component is less energetic, compared to the large-scale component, that the two other flow regimes (Perret, 2019).

Effect of the canopy geometry on model's parameters

The wall-normal evolution of the coefficient Γ and statistics of the universal signal u^* are given in figure 5 for each of the six cases. There is a strong dependence of the Γ coefficient with the canopy geometry, which is more pronounced for $\lambda_p = 44.4\%$, whereas the Reynolds number has little effects (at least in the narrow range of Re_τ studied here). As discussed above, the characteristics of the shear layer in the skimming flow regime change the characteristics of the small-scale structures and their interactions with the large-scale structures in the outer layer above. It is therefore not surprising to find changes in the model's coefficient. The roughness configurations $\lambda_p = 6.25\%$ and $\lambda_p = 25\%$ have a similar Γ coefficient except close to the roughness elements. This dependence on the roughness configuration close to the cubes is a result of changes to the dynamics of the shear layers that develop at the top of the roughness elements in the different flow regimes. Within the skimming flow regime the shear layer does not penetrate the roughness elements resulting in a thin shear layer, whereas the spacing between roughness elements in the isolated wake and wake-interference regimes result in a shear layer that penetrates the canopy layer increasing the vertical transfer of momentum in this region (Basley *et al.*, 2019). The shear layer in a wake-interference flow regime also experiences a strong flapping phenomenon that promotes the transfer of momentum between the canopy layer (small scales) and outer layer (large scales).

The influence of the roughness configuration can also be seen in the profiles of variance and skewness in the inner-layer close to the roughness, whereas this influence becomes negligible in the profile of kurtosis. The changes in variance and skewness are a result of changes to the small-

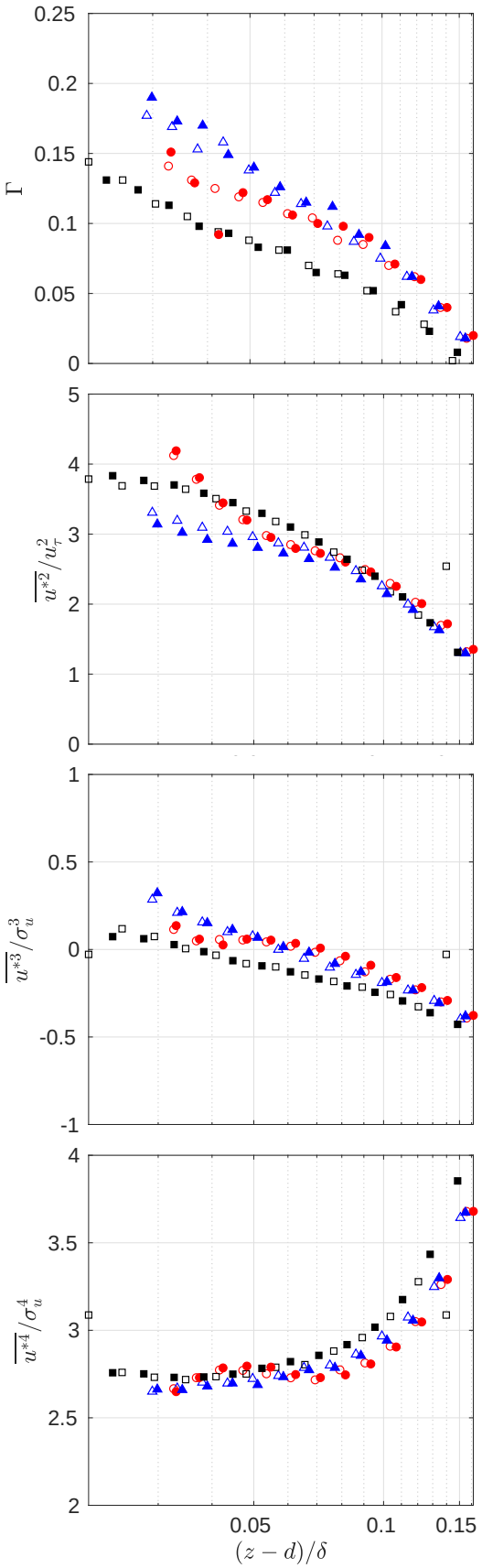

Figure 5. Model's parameters: wall-normal evolution of the coefficient Γ and statistics of the universal signal u^*.

scale structures produced by the roughness. Small-scales in the wake-interference flow regime have larger magnitudes of skewness and smaller magnitudes of turbulence intensity compared to the skimming flow regime.

These results show that the model coefficient and universal signal are significantly influenced by the canopy flow regime. However, Basley *et al.* (2019) have shown that away from the roughness elements the large-scale structures are found to be similar in each configuration. Therefore, the so-called universal signal is not universal for all rough-wall boundary layers and the predictive model must be calibrated for each of the roughness flow regimes.

Prediction and validation

The model and its parameters Γ and u^* obtained above enable the prediction of a statistically representative signal, u_p^+, that hypothetically can be reconstructed at any Reynolds number, where the only required input is the large-scale reference signal, u_L^+. Here, a series of tests are performed in order to assess the capability of the present model, which works well in smooth-wall boundary layer, to be applied in an urban-type boundary layer. Three tests have been chosen, in which canopy configuration and Reynolds numbers are mixed, as seen in Table 2, in order to answer the following questions:

(i) does the model is able to take into account the Reynolds number effect (*i.e.* performing prediction at an higher Reynolds number that the calibration)?

(ii) in what extent the calibration is dependent on the plan area packing density at which the calibration is performed?

(iii) in what extent both Reynolds number and packing density can be combined?

It should be emphasised that for the last question the answer is partially known, and only the packing density of the input large-scale component is varying. Indeed, the differences in the characteristics of the universal signal and the predictive model coefficients prevent the application of a calibrated model at one λ_p to a prediction at another λ_p. The model must be calibrated using measurements from a canopy with the same configuration as the targeted one.

Table 2. Characteristics of the input (calibration parameters and large-scale signal) and output of the predictive model used for testing and validating the prediction capabilities of the model.

Test		Calib.	LS	Pred.
No. 1	λ_p (%)	25	25	25
	Re_τ	32 400	49 900	49 900
No. 2	λ_p (%)	25	6.25 or 44.4	25
	Re_τ	32 400	32 400	32 400
No. 3	λ_p (%)	44.4	25	44.4
	Re_τ	32 400	49 900	49 900

As shown by the error associated with each test in figure 6, there is excellent agreement between the predicted signals and the near-canopy signal for statistics up to the 4^{th} order. The variance is reconstructed with less than 0.3% of error, whereas skewness and kurtosis errors are below 3%. The reconstructed spectra (Fig. 7), shown in figure at the wall-normal location $z/h = 1.25$, also depict an excellent agreement with original (except a slight shift observed on the wavelength for test 1 that may be attributed to the application of Taylor's hypothesis).

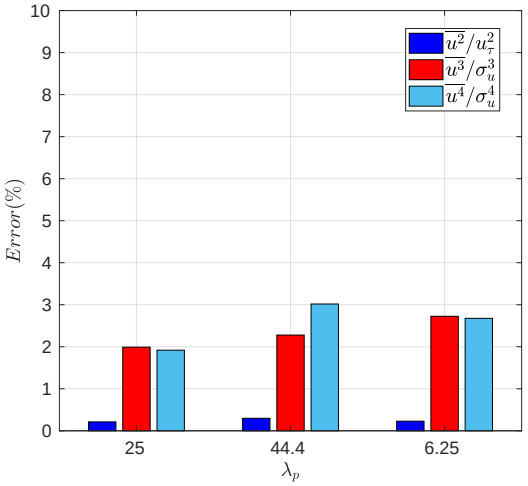

Figure 6. Error of u_p^+ statistics variance, skewness and kurtosis where u_p^+ is determined using model coefficients calibrated at a certain λ_p and u_L^+ at a different λ_p both at $Re_\tau = 32\,400$.

In the smooth wall special attention has been paid to conserving the phase between the universal signal and large-scale signal used to run the predictive model (Mathis, 2011). In these cases the large-scale reference signal used to run the predictive model was adjusted to retain the Fourier phase information of the large-scale signal used to build the universal signal. The phase information of the original large-scale signal is extracted using a Fourier transform and applied to the new large-scale reference signal. This process essentially re-synchronises the new large-scale reference with the universal signal, u^*. For further details refer to Mathis *et al.* (2011). Here, this process was applied before performing the predictions detailed above. To determine influence of the phase shift on a prediction a test is performed using the large-scale reference signal used to build the predictive model. This signal is shifted out of phase with the universal signal and a prediction of the statistics made at each time-shift (Fig 8). As the phase shift increases the estimation of the variance, skewness and kurtosis worsen until they reach a plateau. The effect of the phase shift increases with increasing order of the statistic with the kurtosis showing the largest discrepancy. This suggests that conserving the phase information of the large-scale signal used to calibrate the model is important to the prediction.

CONCLUSION

The predictive model originally introduced by Mathis (2011) for the smooth-wall boundary layer is investigated in the context of urban-type boundary layer. Three roughness arrays consisting of cubical roughness elements with plan area packing densities of 6.25%, 25% and 44.4%, corresponding to the three flow regimes (respectively isolated wake, wake interaction and skimming flows, Grimmond & Oke (1999)) were studied at two freestream velocities and used to determine the influence of both the canopy geom-

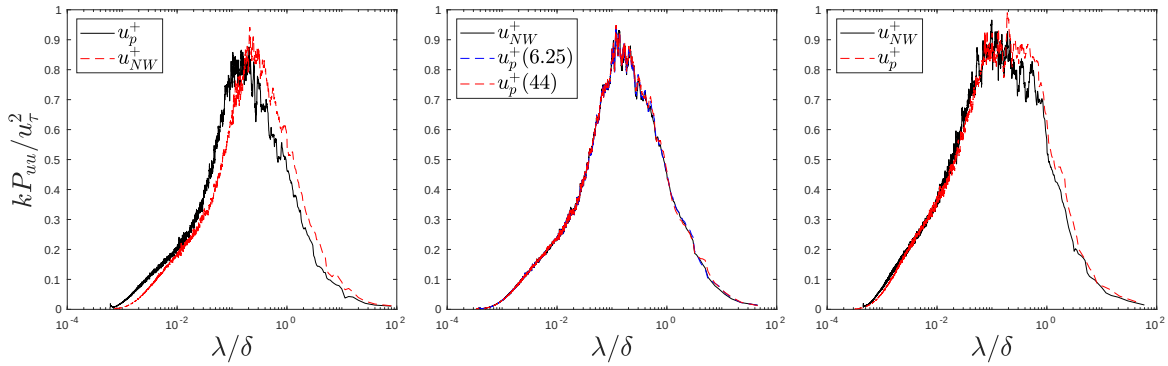

Figure 7. Spectra comparison between the reconstructed signal u_p^+ and the original near-wall signal u_{NW}^+ at $z/h = 1.25$, for *(left)* Test 1, *(centre)* Test 2 and *(right)* Test 3.

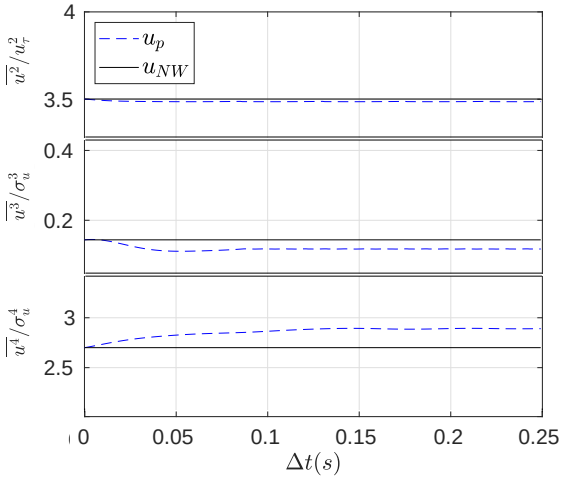

Figure 8. a) Variance, b) skewness and c) kurtosis of u_p^+ and u_{NW}^+ for configuration with $\lambda_p = 25\%$ at $Re_\tau = 32\,400$ using phase shifted large-scale reference signal at $z/h = 2.1$ ($(z-d)/\delta = 0.066$).

etry and Reynolds number on the interaction between the most energetic scales from the outer layer and those in the roughness sublayer. Through analysis of the model's parameters Γ and u^* it is observed that the canopy geometry has a significant influence on scale-interactions as well on the model's parameters. In particular, the skimming flow regime shows higher discrepancy compared to the two other flow regimes. In this case, the dense packing area does not allows the flow to penetrate within the canopy, whereas in the isolated wake and wake interaction regimes the flow penetrates the canopy and a strong shear layer is generated at the top of the cubes. This imply that the model needs to be calibrated for each family of packing density (isolated wake, wake interaction and skimming flows). Through this work it has been demonstrated that the non-linear interactions within urban-type rough-wall boundary layers can be modelled using the predictive model as proposed by Mathis (2011). Although the Reynolds number was shown to have a negligible influence on the model parameters data should be obtained from higher Reynolds number rough-wall flows to expand the range studied.

REFERENCES

Baars, W. J., Hutchins N. Marusic I. 2016 Spectral stochastic estimation of high-reynolds-number wall-bounded turbulence for a refined inner-outer interaction model. *Physical Review Fluids* **1**, 054406.

Baars, W. J., Talluru, K. M., Hutchins, N. & Marusic, I. 2015 Wavelet analysis of wall turbulence to study large-scale modulation of small scales. *Experiments in Fluids* **56** (10), 188.

Basley, Jérémy, Perret, Laurent & Mathis, Romain 2019 Structure of high reynolds number boundary layers over cube canopies. *Journal of Fluid Mechanics* **870**, 460–491.

Blackman, K. & Perret, L. 2016 Non-linear interactions in a boundary layer developling over an array of cubes using stochastic estimation. *Physics of Fluids* **28**, 95–108.

Blackman, K., Perret, L. & Savory, E. 2018 Effects of the upstream-flow regime and canyon aspect ratio on non-linear interactions between a stree-canyon flow and the overlying boundary layer. *Boundary-Layer Meteorology* **1**, 1–22.

Grimmond, C. S. B. & Oke, T. R. 1999 Aerodynamic properties of urban areas derived from analysis of surface form. *Journal of Applied Meteorology* **38**, 1262.

Guala, M., Metzger, M. & McKeon, B. 2011 Interactions within the turbulent boundary layer at high reynolds number. *J. Fluid Mech.* **666**, 576–604.

Mathis, R., Hutchins N. Marusic I. 2009 Large-scale amplitude modulation of the small-scale structures in turbulent boundary layers. *Journal of Fluid Mechanics* **628**, 311–337.

Mathis, R., Hutchins N. Marusic I. 2011 A predictive inner-outer model for streamwise turbulence statistics in wall-bounded flows. *Journal of Fluid Mechanics* **681**, 537–566.

Mathis, R., Marusic, I., Hutchins, N. & Sreenivasan, K. R. 2011 The relationship between the velocity skewness and the amplitude modulation of the small scale by the large scale in turbulent boundary layers **23** (12), 121702.

Perret, L., Basley J. Mathis R. Piquet T. 2019 Atmospheric boundary layers over urban-like terrains: influence of the plan density on the roughness sublayer dynamics. *Boundary-Layer Meteorology* **170**, 205–234.

Squire, D. T., Baars W. J. Hutchins N. Marusic I. 2016 Inner-outer interactions in rough-wall turbulence. *Journal of Turbulence* **17**, 1159–1178.